Electric Field Effects on Insulin Chain-B Conformation

Akin Budi,[†] F. Sue Legge,[‡] Herbert Treutlein,[‡] and Irene Yarovsky*[,†]

Applied Physics, School of Applied Sciences, RMIT University, GPO Box 2476V, Melbourne, Victoria, 3001, Australia, and Cytopia Research Pty. Ltd., PO Box 6492, St. Kilda Road Central, Melbourne, Victoria, 8008, Australia

Received: May 24, 2005; In Final Form: August 16, 2005

The response of proteins to different forms of stress continues to be a topic of major interest, especially with the proliferation of electromagnetic devices conjectured to have detrimental effects on human health. In this paper, we have performed molecular dynamics simulations on insulin chain-B under the influence of both static and oscillating electric fields, ranging from 10^7 to 10^9 V/m. We have found that both variants have an effect on the normal behavior of the protein, with oscillating fields being more disruptive to the structure as compared to static fields of similar effective strength. The application of a static field had a stabilizing effect on the secondary structure, restricting the inherent flexibility that is crucial for insulin's biological activity.

Introduction

The proliferation of radio frequency electromagnetic devices has raised concerns regarding the effects of electric and magnetic radiation on human health. Electromagnetic field exposure is ubiquitous in our everyday life—including occupational, medical, and residential exposure. Some familiar concerns, particularly with respect to children, include close proximity to power transmitters and the rapid increase in the use of mobile phones. While it is generally assumed that the power levels delivered by these devices are small enough to have no ill effect, a recent study has shown evidence of nonthermal microwave damage to brain tissues in exposed rats.[1] The nonthermal effect has also been suggested where microwave radiation altered protein conformation without bulk heating.[2] One of the possible explanations for this nonthermal effect is that the application of pulsed microwave radiation causes a rapid temperature rise that returns to the baseline temperature faster than can be detected by normal thermometry.[3] The temperature rise can alter protein conformation, which in turn can change a protein's activity, causing detrimental effects. For example, changes in protein conformation can induce the formation of amyloid fibrils,[2] a basis for diseases such as Alzheimer's disease, cystic fibrosis, and variant Creutzfeldt−Jakob disease.

There is ongoing debate concerning the true nature of electromagnetic radiation effects on humans. The studies reported in the literature are difficult to interpret and divided in their conclusions (see Ahlbom et al.[4] and references therein). The exact nature and extent of electromagnetic field exposure is extremely difficult to measure. Moreover, the lag-time period of studies thus far is relatively short (regular mobile phone use has only become prevalent in the 1990s) and may not be sufficiently long to cover the period between exposure and disease manifestation. For example, one study reported at least 3-fold increase in acoustic neuroma among users of analogue mobile phones (a common source of electromagnetic radiation), regardless of the induction period.[5] In another more recent study, the researchers concluded that short-term exposure to mobile phones does not increase the risk of acoustic neuroma, although they indicated the possible increase in risk for long-term exposure (at least 10 years in duration) to analogue phones.[6] The specific effects of electric and magnetic field exposure on biological systems have been the subject of a number of investigations showing conflicting results. A study investigating the effect of 50 Hz sinusoidally oscillating magnetic field exposure on human peripheral blood mononuclear cells reported that magnetic field strengths up to 2.5 mT do not affect the activity and proliferation of the cells.[7] On the other hand, another study reported that the exposure of rats to 50 Hz oscillating magnetic field strengths up to 0.1 mT yield depression in pineal serotonin-*N*-acetyltransferase.[8] Similar research using electric fields, however, showed severe alteration to the pineal melatonin content and serotonin-*N*-acetyltransferase[9] and interference in the normal expression of nocturnal melatonin levels in rats.[10] Of some concern is the relatively small number of studies investigating the effects of static magnetic fields, which occur in industrial and medical processes.[11] A review of the available literature covering the biological effects of exposure to magnetic resonance imaging did not find evidence of any health hazard, although it was suggested that there are physical mechanisms of interaction between tissue and magnetic field.[12]

We believe that to gain insight into the nature of the interaction between electromagnetic fields and cells, it is first necessary to examine the mechanistic response of proteins under the influence of the fields at atomistic detail. The time frame of these interactions is very short (within nanoseconds) and thus very difficult to probe experimentally. As a first step to understand the protein response mechanisms to these short-lived stresses, it is useful to examine and compare protein behavior under the influence of an electric field alone and under thermal stress. In a previous study, we have shown that a simultaneous application of chemical and thermal stress disrupts protein conformations to a larger extent than either of the stresses alone.[13] In this paper, we present our study of the protein's response to static and oscillating electric fields of different strengths and compare them to both the behavior of proteins

* Corresponding author. Phone: +61 3 9925 2571; fax: +61 3 9925 5290; e-mail: irene.yarovsky@rmit.edu.au.
[†] RMIT University.
[‡] Cytopia Research Pty. Ltd.

10.1021/jp052742q CCC: $30.25
Published on Web 11/04/2005

under ambient conditions and the behavior of proteins under thermal stress.

We have chosen the insulin hormone for our study due to its biological significance in regulating blood sugars and promoting growth, which has led to numerous studies on the mechanism of insulin's formation and bioactivity.[13−18] Insulin consists of two chains: chain-A with 21 amino acid residues and chain-B with 30 amino acid residues. They are connected by two interchain disulfide bonds between residues A7−B7 and residues A20−B19. In addition, one intrachain disulfide bond exists between residues A6−A11. Although there are known variations in the primary sequence for different species, the tertiary structure of the protein remains well-preserved. On the basis of studies of despentapeptide insulin, which lacks a dimer-forming region, it is believed that the active form of insulin in solution is a monomer.[19] However, obtaining a crystal structure of an intact insulin monomer has proven to be very difficult due to its solubility and self-association.[20] Thus, the structural knowledge of native monomeric insulin has been primarily gained from engineered monomeric insulin.[21]

In this study, we concentrated on the structure of insulin chain-B as there is experimental evidence that it is predominantly stable independently of chain-A.[15,22] Our previous study comparing the effect of chain-B isolation and thermal stress on insulin has also confirmed this property, although increased flexibility was observed in the terminal regions.[13] There are many known conformations of chain-B, defined by the structure of the N-terminus. The main conformations are the R- and T-states.[23] In the R-state, residues B1−B8 are in a helical conformation, while in the T-state, these residues are in an extended conformation. The T-state is thought to be the active state, as it is believed to be the conformation adopted by monomeric insulin.[24] Our previous work has also indicated that a T-like state better satisfies the nuclear magnetic resonance (NMR) experimental data of bovine insulin chain-B in solution, as compared to any other conformations.[18] The present study extends that work by comparing the normal behavior of isolated chain-B with the stress response behavior under the conditions of increased temperature and the application of electric field.

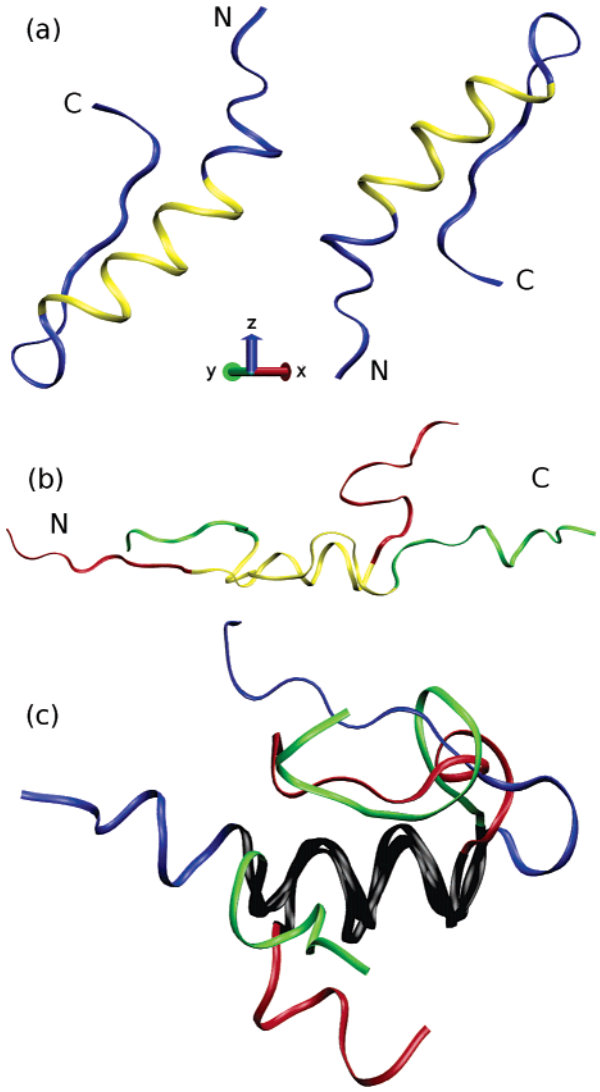

Figure 1. (a) Starting structure of insulin chain-B used in this simulation. The terminal regions have been labeled, and residues B9−B19 have been highlighted in yellow. Different initial orientations with respect to the electric field (applied in the *z*-direction) are shown. (b) Conformations of systems S2 (red) and O2 (green) at the end of the simulation. The residues B9−B19 are highlighted in yellow. (c) Formation of T-like state in systems N300 (red) and O4 (green). The starting structure (R^f-state) is shown in blue. Residues B9−B19 are shown in black.

Materials and Methods

This study utilizes a classical molecular dynamics algorithm[25,26] as implemented in NAMD.[27] The empirical, all-atom CHARMM27 force field[28] was chosen to represent the interactions between atoms. Between 10 and 12 Å, the nonbonded potential function was multiplied by a linearly decaying switching function, which results in zero force field interaction beyond 12 Å. Neighbor list was maintained for atoms within a 14 Å radius.

The SHAKE algorithm[29] was employed to fix the lengths of bonds involving hydrogen atoms to their energy minimized values. This allowed us to ignore vibrational modes of hydrogen bonds and use a longer time step of 2 fs for all the simulations. Particle Mesh Ewald summation was employed to account for long-range electrostatics.[30−32] The starting structure coordinates for each system were taken from the Protein Data Bank.[33] We have chosen the chain-B of wild boar insulin hormone (PDB accession code 1ZNI[34]) for our study. This particular insulin structure has an R^f-form,[14,17] with residues B1−B3 and B24−B30 in extended conformation, residues B4−B19 in α-helical conformation, and residues B20−B23 forming a turn (shown in Figure 1a).

The protein was enclosed in a periodic box sized 60 Å × 60 Å × 60 Å. After filling the box with 7002 TIP3P[35] water molecules (corresponding to water density of 1.0 g/cm^3), the whole system was energy minimized for 20 000 steps by way of conjugate gradient and line search algorithms. Two equilibration stages were then performed successively, each lasting 600 ps at a temperature of either 300 or 400 K. The first of these stages was performed in a constant volume (NVT) ensemble. This was followed by constant pressure (NPT) equilibration at 1 bar, utilizing the Nosé−Hoover method of pressure control in which fluctuations in the barostat are controlled by Langevin dynamics,[36] as implemented in NAMD. The dynamics (data collection) stage was then performed in a constant pressure (NPT) ensemble set to 1 bar with thermal bath coupling to either 300 or 400 K for up to 10 ns. The atomic coordinates were saved every 2500 steps (5 ps) for analysis, resulting in between 340 and 2000 trajectory frames. The validity of this methodology has been confirmed in our previous study,[18] which reproduced the known flexibility of insulin with the majority of the sampled conformations satisfying the nuclear overhauser effect (NOE) distance restraints obtained by NMR spectroscopy.[15]

TABLE 1: Summary of Simulated Systems[a]

system designation	electric field strength (V/m)	temperature (K)	simulation length (ns)
S1, O1	10^9	300	1.7, 3
S2, O2	5×10^8	300	5.9, 3
S3, O3	10^8	300	7.2, 10
S4, O4	5×10^7	300	10, 10
S5, O5	10^7	300	10, 10
N300	0	300	10
N400	0	400	10

[a] The prefix S stands for static field, O for oscillating field, and N for no field.

The summary of the simulated systems is presented in Table 1. We have applied static and oscillating electric fields (denoted by the letters S and O in the system name, respectively) in the same direction (*z*) to the same initial peptide conformation and orientations shown in Figure 1a. Two reference simulations were also performed at temperatures of 300 and 400 K, denoted by the label N300 and N400, respectively. The oscillating electric field was modeled by changing the strength of the field every 20 fs, following a sinusoidal pattern with a frequency of 2.45 GHz (a period of 401.16 ps), which corresponds to the frequency of conventional microwave ovens and wireless and Bluetooth devices. This frequency was used in previous experimental work investigating the effect of microwave radiations on various proteins.[37] As a comparison, digital mobile phones operate at frequencies ranging between 1.8 and 1.9 GHz with the third generation systems using up to 2.2 GHz.

The values of electric field were chosen to cover a range between 10^7 and 10^9 V/m. The highest value corresponds to the value of the electric field where previous molecular dynamics simulations observed structural changes in the water structure.[38]

Results and Discussion

Secondary Structure Analysis. The secondary structure evolution of the systems studied was characterized using the STRIDE algorithm,[39] as implemented in VMD.[40] The results are shown in Figure 2.

Figure 2 shows that the application of oscillating electric field with strengths equal to and above 5×10^8 V/m (systems O1 and O2) in most cases severely disrupts the helical region of the protein, as compared to the application of static fields of similar effective strengths. This can readily be seen in system O1, where all helical content was lost within 1.2 ns (2.8 electric field oscillations), and in system O2, where all helical residues were lost within 2.2 ns (5.3 electric field oscillations). In contrast, systems S1 and S2 retained 37.5 and 69% of the helix, respectively, by the end of the simulations. A comparison of typical sampled structures for systems S2 and O2 is shown in Figure 1b. It is interesting to note that there is a constant transition observed between α-helix and π-helix in system O3, becoming more pronounced as the simulation progresses. The occurrence of π-helices in simulations has been debated recently, with studies suggesting that they may be an artifact of specific force fields.[41] However, the force field investigations were performed under implicit solvent condition, which may not be directly comparable to simulations with explicit solvent. There are also experimental studies indicating that π-helices do occur in a protein's dynamic behavior and play an important role in its normal function.[42,43] In this work, we observed the π-helix in less than 30% of combined simulation time, which indicates that it is not caused by the force field but instead represents a genuine conformational feature.

The active state of insulin is believed to be the T-state, which is characterized by the extended B1−B8 residues.[19] To form this state, it is necessary for insulin in the R- or R^f-state to first break its central helix and then fully extend residues B1−B8. This transition occurs at Gly B8. The glycine residue is well-known as a helix breaker.[44] The event is present in all the systems studied here, except for static field systems S2, S3, and S4. It appears that the application of a strong static electric field interferes with the helix breaking mechanism. In system S1, the helix breaking took place at valine residue B12, known to be important for receptor binding and dimer formation.[45,46] Figure 1c shows the R^f-state of the starting structure and the formation of the T-like state in systems N300 and O4, where the helix splitting at B8 occurred, but residues B4−B7 remained in a helical conformation.

Helical Dipole Moment Distribution. Insulin chain-B possesses a strong dipole moment due to the helical nature of the central region and has the potential to be affected by the application of an electric field. As the electric field is applied, the peptide is induced to align itself with respect to the field. Figure 3 shows the distribution of dipole moment values of the B9−B19 helix in the applied field direction (*z*-axis) for all the systems over the data collection stage. The dipole moment distributions have been normalized to allow direct comparison between different electric field strengths. It can be seen that there is no preferential direction of the helix in the reference (no field) simulations, as expected. The oscillating fields either produce a double peak or a range of values distributed almost symmetrically around zero, where the helix is perpendicular to the electric field. Such distribution of a dipole moment is characteristic of the continuous realignment of the helix with respect to the field. In contrast, the static fields consistently produced preferential alignment of the helix in the direction of the applied field, as illustrated by the well-pronounced peaks of the corresponding dipole moment distributions. Similar geometries and the same dipole moment distributions were obtained for the different initial orientations of the peptide shown in Figure 1a. Moreover, the peaks of the dipole moment distribution of the static field systems coincide with the peaks for oscillating field systems, further confirming that the orientation of the peptide is affected by the field applied rather than its initial orientation. The representative conformations for the systems under applied static electric fields are shown in Figure 4 to demonstrate the observed alignments. The reference systems are also shown for comparison.

PEPCAT Analysis. PEPCAT is a peptide analysis tool that classifies a trajectory into conformational states based on a set of chosen geometric descriptors.[47] In this work, conformational analyses were performed using PEPCAT on systems S4, O4, S5, and O5, along with the reference systems to investigate the conformational dynamics of each system. The systems were selected to examine the more subtle disruption to the secondary structure as compared to the systems at higher field strengths, as evident from Figure 2.

The following PEPCAT descriptors were used to classify the conformations: φ and ψ dihedral angles of residues B8, B18, B19, B20, and B21; contact distance between residues B16 and B24; and distance between α-carbon atoms of residues B5 and B13. The dihedral descriptors were chosen to detect changes in both ends of the B9−B19 central helix; the contact distance was chosen to examine changes at the C-terminal hydrophobic core; and the α-carbon atom distance was chosen to detect the packing direction of the N-terminus.

These descriptors resulted in the classification of the systems into a number of states, which are shown in Table 2. For clarity,

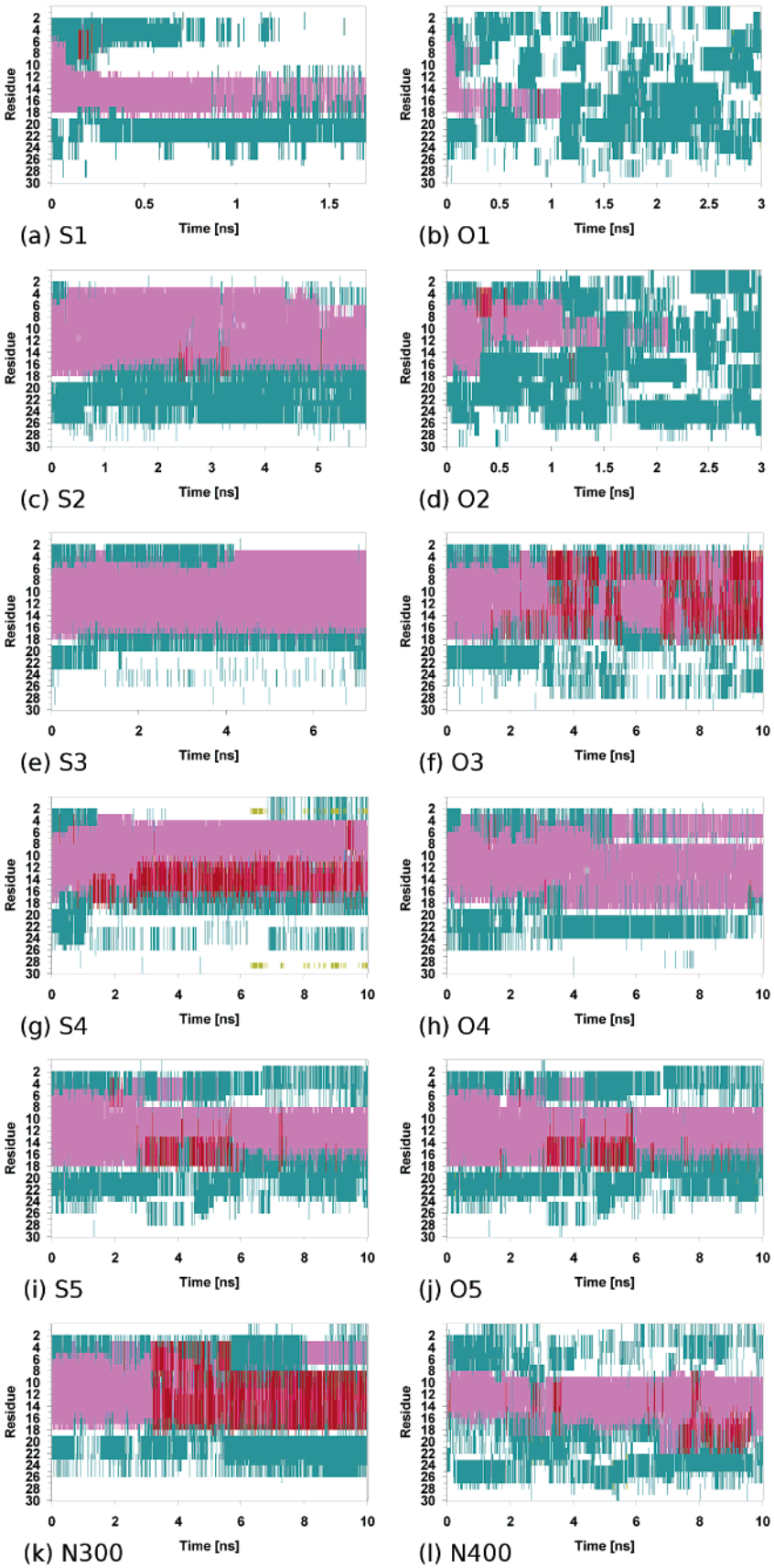

Figure 2. Maps showing the evolution of secondary structure of each system as a function of time. The extent of the time axes corresponds to the simulation lengths shown in Table 1. Dark magenta denotes α-helix, red denotes π-helix, cyan denotes turn, and white denotes coil.

transient conformational states that occupy less than 1% of simulation time have been removed. This preserves more than 85% of the original simulation lengths for all systems except the N400 system, where 67% of the original length was preserved. This illustrates that the system under thermal stress samples a large number of conformational states very efficiently within the time frame of the simulation. Analyses of repeat simulations at 300 K with no applied field (data not shown)

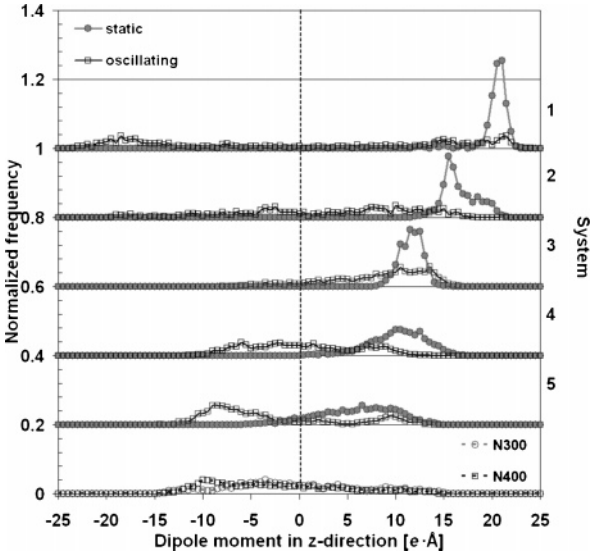

Figure 3. Distribution of the dipole moment of the B9−B19 helix in the *z*-direction. Each plot has been shifted by 0.2 along the *y*-axis.

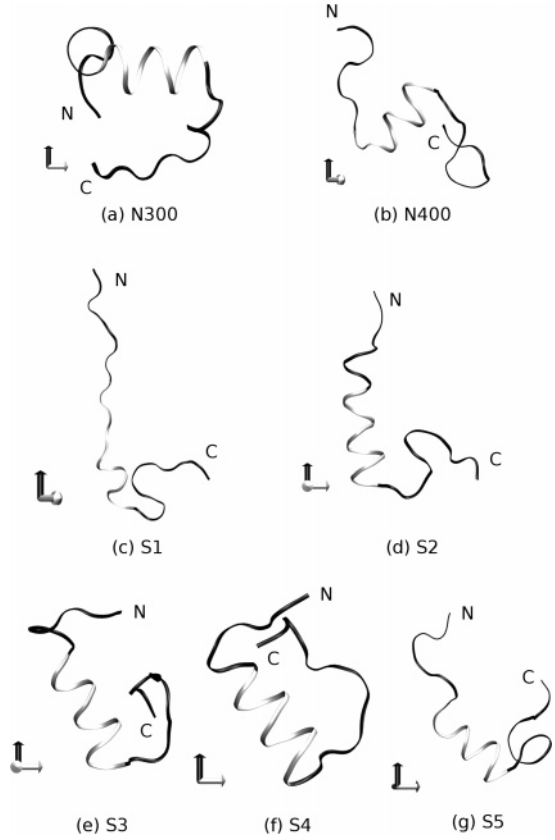

Figure 4. Representative conformations of the reference systems and systems under applied static electric fields at the equilibrium stage of the simulation. Residues B9−B19 are highlighted. The *z*-axis is highlighted in black.

demonstrated that the systems spent more than 80% of simulation time in conformational states shared with the N400 system, thus confirming that the N400 system efficiently sampled a large number of the conformational states available at ambient conditions (300 K systems with no applied field). This finding is further supported by the low percentage of simulation time (less than 6%) spent by these systems outside the conformational states shared with the reference systems.

All systems under electric field stress were shown to spend more time in conformational states sampled by system N400 rather than by system N300. This indicates that the time evolution of the system under electric field stress has more in common with a system under thermal stress than under ambient conditions. However, these systems also spent a large amount of time (up to 20%) in conformational states not observed in either of the reference systems. This behavior is more prominent in the systems with higher electric field strength, suggesting that the mechanism of interaction between the electric field and a protein differs from the interaction resulting from the thermal stress alone. It is interesting to note that there is a relatively low number of states that exhibit deviation from normal conformations accessible to the reference systems. For example, in system S4, there is only one identified state outside the range of conformational states sampled by the reference systems, yet it accounts for more than 21% of the simulation time.

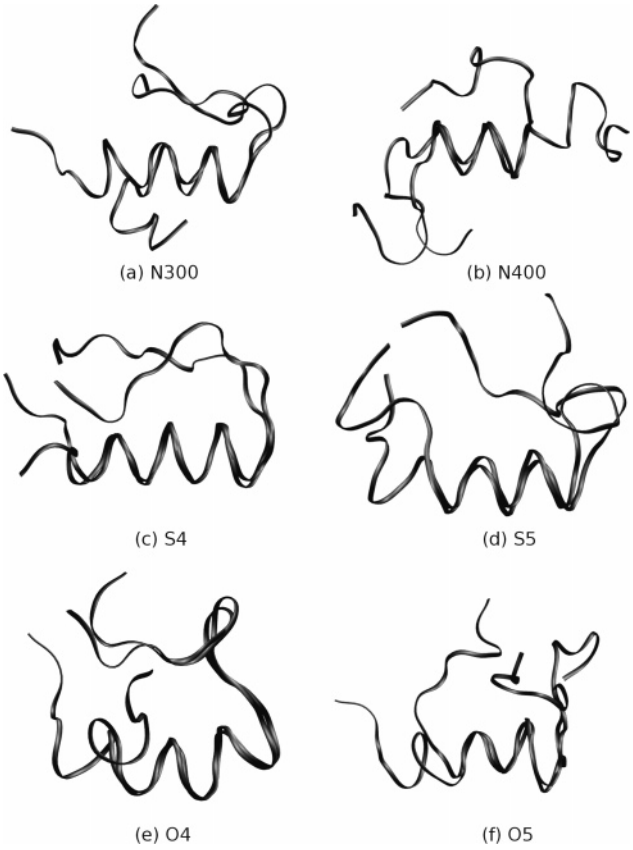

Figure 5. Two most occupied states for selected systems. Oscillating systems undergo a conformational change in the C-terminal region.

In terms of differences between the effect of static and oscillating fields of the same strength, the oscillating field systems were observed to spend more time in conformational states sampled by the N300 system as compared to the static field systems. This may be due to the brief relaxation periods experienced by the systems under applied oscillating field as the electric field reverses its direction. In addition, a stronger electric field in both systems was shown to decrease the time spent in conformational states sampled by the N300 system, although the time spent in conformational states sampled by the N400 system is relatively unaffected. As there is an overlap between the states sampled by both reference systems, this can be explained by the electric field systems moving out from the local potential energy minima sampled by the N300 system.

Figure 5 shows the graphical representation of the two most occupied conformational states in the systems chosen for PEPCAT analysis. The figure shows that the highest occupied state in system N300 is a T-like structure, stabilized by the

TABLE 2: Comparison of Sampled States for Systems Chosen for PEPCAT Analysis with Systems N300 and N400

system	electric field strength (V/m)	no. of sampled states	percentage of time spent within states occupied by system N300	percentage of time spent within states occupied by system N400	percentage of time spent outside states occupied by systems N300 and N400
N300	0	9	100	49.3	0
N400	0	30	6.0	100	0
S4	5×10^7	7	18.8	74.6	21.0
O4	5×10^7	18	32.4	72.4	14.6
S5	10^7	19	43.3	76.7	13.4
O5	10^7	12	70.6	83.1	11.3

TABLE 3: B9−B19 Backbone RMSD of the Helix of Each Simulation, Averaged Over the Last 1 ns of the Data Collection Stage

static fields	RMSD (Å)	oscillating fields	RMSD (Å)	ref systems	RMSD (Å)
S1	2.9 ± 0.2	O1	4.72 ± 0.55	N300	2.25 ± 0.08
S2	1.5 ± 0.2	O2	4.33 ± 0.35	N400	1.5 ± 0.6
S3	1.51 ± 0.15	O3	2.2 ± 0.1		
S4	2.26 ± 0.09	O4	1.41 ± 0.15		
S5	1.57 ± 0.15	O5	1.9 ± 0.4		

TABLE 4: Radius of Gyration of Each Simulation, Averaged Over Data Collection Stage, After the First 1 ns

static fields	R_g (Å)	oscillating fields	R_g (Å)	ref systems	R_g (Å)
S1	15.7 ± 0.3	O1	13 ± 2	N300	9.7 ± 0.5
S2	11.2 ± 0.3	O2	13.8 ± 1.7	N400	11.0 ± 1.3
S3	10.1 ± 0.3	O3	10.9 ± 0.8		
S4	10.1 ± 0.4	O4	9.9 ± 0.5		
S5	10.5 ± 0.8	O5	10 ± 1		

TABLE 5: Number of Retained Helical Residues, Averaged Over Data Collection Stage

static fields	no. of residues in helix	oscillating fields	no. of residues in helix	ref systems	no. of residues in helix
S1	5.8 ± 2.6	O1	1.5 ± 2.8	N300	11.4 ± 2.7
S2	12.7 ± 1.7	O2	3.9 ± 4.2	N400	8.8 ± 2.4
S3	12.6 ± 1.3	O3	11.8 ± 2.2		
S4	12.3 ± 1.3	O4	12.8 ± 2.3		
S5	9.9 ± 2.6	O5	9.5 ± 1.9		

formation of a hydrogen bond between residues B5 and B13 that persists up to the end of the simulation time frame. This conformational feature has been discussed in a previous study of insulin.[18] In system N400, extreme flexibility on both terminal regions was observed,[13] with secondary structure disruption particularly prominent in the N-terminal region. The C-terminus was also observed to move away from the main B9−B19 helix, exposing the hydrophobic core region of the protein.

The systems under applied static electric field (Figure 5c,d) preserve most of their α-helical region and exhibit less flexibility on both termini regions as compared to the N300 system. This α-helix preservation effect is exaggerated in the systems with a stronger static electric field (refer to Figure 2c,e) and may result from the coupling of the helical dipole moment with the electric field, as illustrated in Figure 3. In contrast to the systems under applied static field, the systems under applied oscillating electric field (Figure 5e,f) showed more flexibility in both termini regions as compared to any other system except the N400. A probable explanation is the added stress to the protein caused by the constant realignment with respect to the direction of the oscillating electric field.

Structural Properties. The structural stability of the B9−B19 helical region under the influence of the applied fields was investigated by determining the root-mean-square deviation (RMSD) as compared to the start of the data collection stage. The average RMSD values for the last 1 ns of the simulations are shown in Table 3. Interestingly, the RMSD of the reference system at 300 K is higher than that for the system at 400 K. This is probably due to the B9−B19 helix adopting a π-helix conformation at 300 K, which was preserved until the end of the simulation.

The observed high mobility of the helical region of the protein at 300 K is related to the inherent flexibility of the isolated insulin chain-B, as discussed previously.[13,18] Similar flexibility was also observed in systems S4 and O3, both of which have comparable RMSD to the reference system at 300 K and exhibited a structural transition toward π-helix (refer to Figure 2f,g). Systems S1, O1, and O2 showed either partial or complete loss of the helical region and thus produced much larger RMSDs. All the other systems have the B9−B19 α-helical region mostly preserved and hence have relatively low RMSDs. The variance in the N400 system showed a relatively high value due to the constant transition between α- and π-helix near the end of the simulation. The variance of the systems under applied oscillating field was also shown to be generally greater than the variance of systems under applied static field of comparable strength and reflects the constant conformational change experienced by the protein as it realigns with respect to the electric field direction.

The radius of gyration (R_g) in each simulation is shown in Table 4. It can be readily seen that all the simulations resulted in a larger R_g as compared to the reference system at 300 K. Systems under static electric field stress did not exhibit significant deviation from the values obtained for the reference structures until a field strength of 10^9 V/m was reached. In contrast, the oscillating field disrupted the protein conformation significantly at the lower effective field strength of 5×10^8 V/m. The variance for the systems under applied static field was shown to decrease as the field strength increases. This agrees with previous analysis suggesting a stronger coupling between the helical dipole moment of the protein with the applied electric field at higher field strengths. This dipole moment coupling limits the conformations that can be accessed by the protein, as evident from Table 2, where system S4 adopts seven conformational states as compared to system S5 with 19 states sampled. On the contrary, systems under applied oscillating field showed increasing variance as the field strength increases. Again, this is due to the protein constantly realigning with respect to the changing field direction.

Table 5 shows the number of retained helical residues calculated using the STRIDE algorithm,[39] as a measure of the stability of the helix over the data collection stage. Systems under moderate static electric field (S2, S3, and S4) showed a slightly larger number of retained helical residues as compared to the reference system at 300 K. This is indicative of the helix stabilization caused by the coupling of the helix dipole with the applied electric field. This helix stabilization is also observed in the O4 system, although the fluctuation is significantly larger than in the systems under applied static fields. Significant

TABLE 6: Percentage of Solvent Accessible Surface Area throughout the Data Collection Stage, Relative to the N300 Simulation

static fields	percentage change of SASA	oscillating fields	percentage change of SASA	ref systems	percentage change of SASA
S1	123.6 ± 1.6	O1	118.8 ± 7.8	N300	100.0 ± 5.8
S2	106.9 ± 2.4	O2	120.9 ± 8.3	N400	107.7 ± 6.6
S3	100.5 ± 2.2	O3	107.7 ± 6.1		
S4	103 ± 6	O4	100.7 ± 4.4		
S5	106.7 ± 4.4	O5	105.1 ± 6.4		

disruption to the helical content was observed at the highest field strength in the static case and in the two highest field strengths in the oscillating case, which is consistent with the observations of the radius of gyration. It is interesting to note that the simulations at electric field of 10^7 V/m (S5 and O5) exhibited a similar number of retained helical residues to the 400 K system. In particular, these systems show some similarities with the secondary structure map (Figure 2i,j,l), both of which show the complete loss of the B4−B8 helix within 5 ns of the simulations.

The solvent accessible surface area (SASA) of the protein was calculated using the program X-PLOR[48] for the whole data collection stage after the first nanosecond of the simulation. For clarity, the resulting SASA and variance are expressed as a percentage of the SASA of the N300 system and are presented in Table 6. The results show that for the systems under applied static fields, although the SASA did not change noticeably up to field strength of 5×10^8 V/m, the variance dropped significantly from a field strength of 10^8 V/m. This indicates the severe restriction of the mobility of the protein under applied static electric field. In contrast, the application of oscillating field severely disrupts the secondary structure at lower field strength of 5×10^8 V/m and exhibits a large variance. This finding is consistent with the other results presented previously and highlights the different mechanism by which the static and oscillating electric fields can cause disruption to the normal protein behavior.

Conclusion

In this work, we have explored and compared the effect of static and oscillating electric fields of different strengths on the behavior of the helical region of insulin chain-B. Our results indicate that the application of oscillating electric fields have a more destabilizing effect on a protein's conformation than a static electric field of the same effective strength. An oscillating field was shown to cause complete loss of secondary structure at a lower field strength as compared to the static electric field, suggesting that the rapid change in electric field direction does more damage to the secondary structure than the application of a fixed electric field.

Moderate strength static fields were observed to have a stabilizing effect on some regions of the secondary structure due to the coupling of the helical dipole moment with the applied field. This coupling can immobilize the inherently flexible regions and restrict the occurrence of specific conformational changes, which can include the biologically active conformations, as observed in our study of the insulin hormone.

Acknowledgment. The authors acknowledge the Australian Research Council (ARC) for the funding necessary for this project. We also acknowledge the Australian Partnership for Advanced Computing (APAC) and the Victorian Partnership for Advanced Computing (VPAC) for the grant of computer time on their supercomputers.

References and Notes

(1) Salford, L. G.; Brun, A. E.; Eberhardt, J. L.; Malmgren, L.; Persson, B. R. R. *Environ. Health Perspect.* **2003**, *111*, 881.
(2) de Pomerai, D. I.; Smith, B.; Dawe, A.; North, K.; Smith, T.; Archer, D. B.; Duce, I. R.; Jones, D.; Candido, E. P. *FEBS Lett.* **2003**, *543*, 93.
(3) Laurence, J. A.; French, P. W.; Lindner, R. A.; McKenzie, D. R. *J. Theor. Biol.* **2000**, *206*, 291.
(4) Ahlbom, A.; Green, A.; Kheifets, L.; Savitz, D.; Swerdlow, A. *Environ. Health Perspect.* **2004**, *112*, 1741.
(5) Hardell, L.; Hallquist, A.; Mild, K. H.; Carlberg, M.; Påhlson, A.; Lilja, A. *Eur. J. Cancer Prevention* **2002**, *11*, 377.
(6) Lönn, S.; Ahlbom, A.; Hall, P.; Feychting, M. *Epidemiology* **2004**, *15*, 653.
(7) Capri, M.; Pietro, M.; Remondini, D.; Carosella, S.; Pasi, S.; Castellani, G.; Franceschi, C.; Bersani, F. *Phys. Biol.* **2004**, *1*, 211.
(8) Selmaoui, B.; Touitou, Y. *Life Sci.* **1995**, *57*, 1351.
(9) Wilson, B. W.; Anderson, L. E.; Hilton, D. I.; Phillips, R. D. *Bioelectromagnetics* **1981**, *2*, 371.
(10) Reiter, R. J.; Anderson, L. E.; Buschbom, R. L.; Wilson, B. W. *Life Sci.* **1988**, *42*, 2203.
(11) Feychting, M.; Ahlbom, A.; Kheifets, L. *Ann. Rev. Public Health* **2005**, *26*, 165.
(12) Formica, D.; Silvestri, S. *BioMed. Eng. OnLine* **2004**, *3*, 11.
(13) Budi, A.; Legge, S.; Treutlein, H.; Yarovsky, I. *Eur. Biophys. J. Biophys. Lett.* **2004**, *33*, 121.
(14) Ciszak, E.; Beals, J. M.; Frank, B. H.; Baker, J. C.; Carter, N. D.; Smith, G. D. *Structure* **1995**, *3*, 615.
(15) Hawkins, B.; Cross, K.; Craik, D. *Intl. J. Peptide Protein Res.* **1995**, *46*, 424.
(16) Derewenda, U.; Derewenda, Z.; Dodson, E. J.; Dodson, G. G.; Reynolds, C. D.; Smith, G. D.; Sparks, C.; Swenson, D. *Nature* **1989**, *338*, 594.
(17) Whittingham, J. L.; Chaudhuri, S.; Dodson, E. J.; Moody, P. C. E.; Dodson, G. G. *Biochemistry* **1995**, *34*, 15553.
(18) Legge, F. S.; Budi, A.; Treutlein, H.; Yarovsky, I. *Biophys. Chem.* **2005**, *118*, 140.
(19) Jørgensen, A. M. M.; Olsen, H. B.; Balschmidt, P.; Led, J. J. *J. Mol. Biol.* **1996**, *257*, 684.
(20) Olsen, H. B.; Ludvigsen, S.; Kaarsholm, N. C. *Biochemistry* **1996**, *35*, 8836.
(21) Hua, Q.-X.; Hu, S.-Q.; Frank, B. H.; Jia, W. H.; Chu, Y.-C.; Wang, S.-H.; Burke, G. T.; Katsoyannis, P. G.; Weiss, M. A. *J. Mol. Biol.* **1996**, *264*, 390.
(22) Qiao, Z.-S.; Min, C.-Y.; Hua, Q.-X.; Weiss, M. A.; Feng, Y.-M. *J. Biol. Chem.* **2003**, *278*, 17800.
(23) Kaarsholm, N. C.; Ko, H.-C.; Dunn, M. F. *Biochemistry* **1989**, *28*, 4427.
(24) Hua, Q. X.; Weiss, M. A. *Biochemistry* **1991**, *30*, 5505.
(25) Allen, M. P.; Tildesley, D. J. *Computer Simulation of Liquids*; Oxford University Press: New York, 1989.
(26) Leach, A. R. *Molecular Modeling: Principles and Applications*, 2nd ed.; Prentice Hall: Harlow, UK, 2001.
(27) Kalé, L.; Skeel, R.; Bhandarkar, M.; Brunner, R.; Gursoy, A.; Krawetz, N.; Phillips, J.; Shinozaki, A.; Varadarajan, K.; Schulten, K. *J. Comput. Phys.* **1999**, *151*, 283.
(28) MacKerell, A. D., Jr.; Bashford, D.; Bellott, M.; Dunbrack, R. L., Jr.; Evanseck, J. D.; Field, M. J.; Fischer, S.; Gao, J.; Guo, H.; Ha, S.; Joseph-McCarthy, D.; Kuchnir, L.; Kuczera, K.; Lau, F. T. K.; Mattos, C.; Michnick, S.; Ngo, T.; Nguyen, D. T.; Prodhom, B.; Reiher, W. E., III; Roux, B.; Schlenkrich, M.; Smith, J. C.; Stote, R.; Straub, J.; Watanabe, M.; Wiórkiewicz-Kuczera, J.; Yin, D.; Karplus, M. *J. Phys. Chem. B* **1998**, *102*, 3586.
(29) Ryckaert, J.-P.; Ciccotti, G.; Berendsen, H. J. C. *J. Comput. Phys.* **1977**, *23*, 327.
(30) Darden, T.; York, D.; Pedersen, L. *J. Chem. Phys.* **1993**, *98*, 10089.
(31) Essmann, U.; Perera, L.; Berkowitz, M. L.; Darden, T.; Lee, H.; Pedersen, L. G. *J. Chem. Phys.* **1995**, *103*, 8577.
(32) Petersen, H. G. *J. Chem. Phys.***1995**, *103*, 3668.
(33) Berman, H. M.; Westbrook, J.; Feng, Z.; Gilliland, G.; Bhat, T. N.; Weissig, H.; Shindyalov, I. N.; Bourne, P. E. *Nucleic Acids Res.* **2000**, *28*, 235.
(34) Bentley, G.; Dodson, E.; Dodson, G.; Hodgkin, D.; Mercola, D. *Nature* **1976**, *261*, 166.
(35) Jorgensen, W. L.; Chandrasekhar, J.; Madura, J. D.; Impey, R. W.; Klein, M. L. *J. Chem. Phys.* **1983**, *79*, 926.
(36) Feller, S. E.; Zhang, Y. H.; Pastor, R. W.; Brooks, B. R. *J. Chem.Phys.* **1995**, *103*, 4613.
(37) Berry, Y. C., personal communication.

(38) Xu, D.; Phillips, J. C.; Schulten, K. *J. Phys. Chem.* **1996**, *100*, 12108.

(39) Frishman, D.; Argos, P. *Proteins: Struct., Funct.,Genet.* **1995**, *23*, 566.

(40) Humphrey, W.; Dalke, A.; Schulten, K. *J. Mol. Graphics* **1996**, *14*, 33.

(41) Feig, M.; MacKerell, A. D., Jr.; Brooks, C. L. *J. Phys. Chem. B* **2003**, *107*, 2831.

(42) Armen, R.; Alonso, D. O. V.; Daggett, V. *Protein Sci.* **2003**, *12*, 1145.

(43) Fodje, M. N.; Al-Karadaghi, S. *Protein Eng.* **2002**, *15*, 353.

(44) Okamoto, Y.; Hansmann, U. H. E. *J. Phys. Chem.***1995**, *99*, 11276.

(45) Hu, S.-Q.; Burke, G. T.; Schwartz, G. P.; Ferderigos, N.; Ross, J. B. A.; Katsoyannis, P. G. *Biochemistry* **1993**, *32*, 2631.

(46) Nakagawa, S. H.; Tager, H. S.; Steiner, D. F. *Biochemistry* **2000**, *39*, 15826.

(47) O'Donohue, M. F.; Minasian, E.; Leach, S. J.; Burgess, A. W.; Treutlein, H. R. *J. Comput. Chem.* **2000**, *21*, 446.

(48) Brünger, A. T. *X-PLOR, Version 3.1: A system for X-ray crystallography and NMR*; Yale University Press: New Have n, CT, 1992. n, CT, 1992.